



SLUG FLOW REGIME IDENTIFICATION FROM DYNAMIC VOID FRACTION MEASUREMENTS IN VERTICAL AIR–WATER FLOWS

G. COSTIGAN and P. B. WHALLEY

Department of Engineering Science, University of Oxford, Oxford OX1 3PJ, U.K.

(Received 5 January 1996, in revised form 3 July 1996)

Abstract—An existing design of conductivity probe for the measurement of void fraction has been developed and tested. Calibration checks showed that the time averaged output of the instrument was close to linear over the whole range of void fraction, with a tendency to overestimate the true value. Computer modelling of the probe's response to different void distributions supported the calibration results. Two meters were used to examine the dynamic variation of void fraction in air–water flows in a vertical 32 mm diameter tube. Flow patterns ranging from bubbly to annular were observed. Examination of the void fraction traces and their probability distribution functions enabled the identification of six flow regimes: discrete bubble flow, spherical cap bubble flow, stable slug flow, unstable slug flow, churn flow and annular flow. The locations of flow regime transition boundaries on a flow pattern map, deduced from this objective analysis, are in agreement with the data of other workers. The unstable slug flow regime corresponds to a region some workers have identified as churn flow, it provides explanations for some of the apparent anomalies concerning the location of the slug to churn flow boundary. Cross-correlation of the signals from the two probes has provided statistical data on the lengths of slugs and Taylor bubbles which suggested modifications to the previous theories enabling the entry to and exit from the unstable slug flow regime to be predicted. © 1997 Elsevier Science Ltd. All rights reserved.

Key Words: slug flow, flow regimes, void fraction, measurements, vertical flow, air and water

1. INTRODUCTION

The work reported here is part of a collaborative programme aimed at defining flow regime transition boundaries in vertical gas–liquid flows with more precision. Within this collaboration, the authors' primary objective is to study the slug to churn transition, but the data presented cover flow patterns from bubbly to annular and the measurement techniques and results are of general interest.

1.1. The slug–churn transition debate

There is a history of uncertainty over the correct location of the slug to churn flow boundary and this uncertainty persists to date.

Taitel *et al.* (1980) argued that slug to churn transition is an entry length effect and that the possibility of observing slug flow depends upon the flow velocities, the tube diameter and the position at which the observation is made. They developed an expression to establish the transition boundary. This predicts that, for air and water in a given tube diameter, the gas velocity corresponding to transition is almost constant as the liquid velocity increases, until, at liquid velocities between 0.1 and 1 m/s it begins to fall. They define churn flow as occurring when oscillatory motion of the liquid is observed. But a number of the data points that they identify as slug flow (for tubes of 25.4 and 50.8 mm diameters) fall to the right of their transition line. This is true also for data from 4 and 12.3 mm diameter tubes reported by Barnea *et al.* (1983). Fernandes *et al.* (1983) show their own data from a 50.8 mm diameter tube on a Taitel flow map. Bubble, slug and churn data points are clearly identified, but no data points are reported from the high liquid velocity region between their slug and churn data.

Bauner and Barnea (1986) developed a slug to churn transition criterion based upon a relationship between the mixture velocity and void fraction at the dispersed bubble flow boundary. For a given maximum limiting void fraction, the dispersed bubble flow boundary mixture velocity

can be calculated. They claimed that this mixture velocity then defines the locus of points of constant void fraction, which represents the slug to churn transition boundary. They selected a maximum slug void fraction of 0.52, the maximum cubic lattice packing fraction. This shows similar trends to lower critical gas velocities as the liquid velocity increases, but again much of their data, identified as slug flow, falls to the right of this line, with churn flow data between it and annular flow. McQuillan and Whalley (1985) and Bilicki and Kestin (1986) proposed criteria for the slug to churn (which Bilicki calls "froth") transition, based upon different mechanisms, but which show similar trends to those already discussed. Wang *et al.* (1991) show churn data from a 50.8 mm tube to the right of the Taitel flow map boundary. But they defined churn flow data as existing when "the integrity of the Taylor bubble is destroyed".

Mishima and Ishii (1984) proposed a transition criterion, which is based upon the mean void fraction becoming equal to the slug void fraction, this predicts that the critical gas velocity will increase with increasing liquid velocity and agrees well with some data for the transition to churn flow. However, a number of workers (McQuillan and Whalley, and Jayanti and Hewitt) have pointed out inconsistencies in this criterion.

Jayanti and Hewitt (1992) considered the slug to churn transition in relation to seven transition to churn data points, observed in a long, 32 mm diameter tube with air and water at 2.4 bar. They pointed out that the data points show an increase in transition gas velocity with water velocity, and concluded that "the model of McQuillan and Whalley is also not consistent with the data". They accepted the basic premise of the McQuillan and Whalley model which is that the slug to churn flow transition is caused by flooding of the liquid film in a Taylor bubble, but modified the calculation so that it predicts increasing critical gas velocities as the liquid flow increases.

Mao and Dukler (1993) questioned the existence of churn flow, by citing experiments in a 50.6mm diameter tube, which gave the visual appearance of churn flow, but which, they claimed, exhibited all of the characteristics of slug flow from radio frequency probe measurements.

Recently Jayanti *et al.* (1993) obtained photographic evidence of the occurrence of flooding waves on the liquid film of a Taylor bubble in a 10 mm diameter tube. They cite this evidence in support of the view that flooding is the cause of the slug to churn transition.

Leaving aside for the moment the question of which transition criterion is "correct", we can conclude that many observers believe that disruption of the slug flow pattern begins at lower gas velocities when the liquid flow is high (say above about 0.3 m/s superficial velocity), than it does when the liquid flow is lower. After this transition there is evidence suggesting the existence of a region at higher gas velocities which, whilst oscillating, still exhibits characteristics of slug flow.

Other workers believe that the churn flow boundary moves to higher gas velocities as the liquid flow increases. Data to the left of this line are either designated slug flow or are ignored.

Thus no consensus exists about the position of the slug flow boundary at higher liquid flows, and there is considerable uncertainty over what flow pattern is being observed: even to the extent of some workers doubting the existence of churn flow.

1.2. Void fraction measurement

The void fraction is a fundamental quantity in the description and analysis of two phase flows; in the case of slug and churn flows the void fraction at any point varies dramatically with time, therefore, a continuous record of void fraction is desirable to describe the flow.

One of the simplest techniques used to determine void fraction is the quick-closing valve method (Nicklin and Davidson 1961). Local void fraction measurements in the bubble and slug flow regimes can be made using a resistance (or conductance) probe (Malnes 1966; Serizawa 1974). Similar measurements can be made by a technique which utilises the change in refractive index, which occurs when a fibre optical probe tip is immersed in a gas or a liquid (Danel and Delhaye 1971; van Hout *et al.* 1992; Spindler 1994). Local methods can give information about the spatial distribution of void fraction, if the probe is traversed in the test section. Radiation attenuation techniques have also been used to measure voidage (Jones and Zuber 1975). Vince and Lahey (1982) made similar, chordal average measurements on a vertical, 25.4 mm diameter tube using X rays. Multi-beam gamma densitometers have also been developed for void fraction measurements in large diameter pipes (Kondic and Lassahn 1978). Kosaly *et al.* (1982) showed the evolution of void fraction PDFs for the bubbly to slug flow transition, by analysing the fluctuating signals

from neutron detectors in a graphite reactor core, in which a two phase flow test section was installed. A gradual transition from a single PDF peak at low void fraction for bubbly flow to a double peaked distribution for slug flow is evident from the data presented by Albrecht *et al.* (1982).

Ma *et al.* (1991) described two methods of measuring void fraction. An impedance probe was connected to a signal processing circuit which gave a linearised output with a fast response. When the void fraction measured by this arrangement was compared with that deduced from fast closing valves, the results agreed to within 20%. They also deduced void fractions below 0.8 to within 20% by measuring the static pressure in a vertical test section and assuming that the total pressure drop was dominated by it. Wang *et al.* (1991) report on the use of this impedance probe to determine flow pattern transitions for air and water in vertical 50.8 mm diameter tubes.

2. VOID METER TESTING AND CALIBRATION

2.1. Impedance void fraction probe

The impedance probe described by Ma *et al.* (1991) and used by Wang *et al.* (1991) is a relatively simple, cheap method of producing a continuous signal which is related to area averaged void fraction, therefore two of these probes were built to fit into the Oxford University vertical air–water test section. This consists of a 32 mm diameter transparent acrylic tube which is approximately 8.5 m high. The probe construction is shown in figure 1.

Two signal processing circuits were also built, generally similar to those described by Ma *et al.* The probe outputs were taken to the signal processing circuits, whose outputs could be either displayed on an oscilloscope or recorded using a high speed data logger.

The voltage output of the probe–circuit combination was initially assumed to be linear with void fraction. Since resistance and capacitance are both functions of void distribution, the validity of this assumption was checked by calibration tests and computer modelling of the probe's response to various void distributions.

2.2. Void meter performance

Water temperature variations had a significant effect on the meter output, suggesting that it was primarily measuring the conductance, rather than the capacitance, of the air–water mixture.

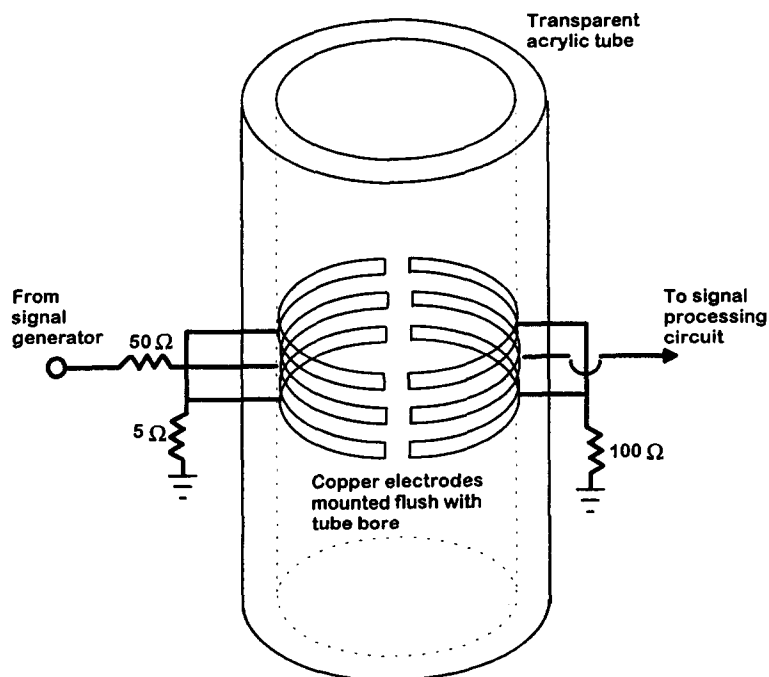


Figure 1. Void fraction conductivity probe arrangement.

Neither Ma nor Wang mentioned any sensitivity of the probe to temperature. Merilo *et al.* (1977), and other workers have used reference circuits to measure and account for this type of behaviour. However, we compensated for the effect during data processing, by using the measured water temperature. More detailed measurements confirmed that the probe was primarily responding to conductivity (Costigan and Whalley 1996). The meters were intended to provide a dynamic record of void fraction. Since no other convenient, reliable and readily available means of making dynamic measurements exists at present, it was necessary to assess their performance by comparison with average void fraction measurements.

Low and zero liquid flow runs were used to compare the time averaged void fraction measured by each meter, with values deduced from the two phase "level swell". A static, vertical column of liquid in a tube has a "collapsed" level L_c , if gas is allowed to flow through this column, the two phase mixture height rises to L_s , determined by the mean density (ρ_m) of the mixture. If the gas flow is low, the pressure drop in both cases is equal to the static head and the mean void fraction (ϵ) is given by:

$$\epsilon = 1 - \left(\frac{L_c}{L_s} \right). \quad [1]$$

The collapsed liquid level was derived from the output of a pressure transducer at the test section inlet, and the two phase level was either measured directly from the tube, or was the overall tube height. The time averaged void meter measurements were then compared with the values corresponding to their heights.

The "level swell" technique described above is only reliable at low liquid flows where the static component of the total pressure drop is dominant. Therefore a modification of the quick closing valve arrangement was used to check the void fractions measured at higher liquid flows. A large bore plastic ball valve was fitted to a rigid mounting near the top of the test section. Two 12 mm bore solenoid valves were fitted near the test section inlet, one in the air supply pipe and the other in the water supply. A micro-switch, attached to the ball valve, shut the solenoid valves within 3 ms when the ball valve handle was moved toward the closed position. The average void fraction from these quick-closing valve measurements was generally slightly lower than the true value (Costigan and Whalley 1996). Repeated measurements at the same conditions showed that the results were usually reproducible to within 0.01, with occasional differences as high as 0.03.

A comparison of the time averaged void fractions from both void meters with level swell and quick-closing valve measurements is given in figure 2. Both meters perform similarly over the full range of void fraction, with C2 indicating slightly higher values than C1. The data have been corrected for static pressure variations, therefore this slight discrepancy is thought to be a characteristic of the meters.

Most of the data points fall between a linear relationship and a curve deduced from Maxwell's (1873) equation for a homogeneous dispersion of small spheres in a continuous medium of different conductivity. If the void meter voltage output is directly proportional to the conductivities of the full tube and of the two phase mixture, then Maxwell's equation predicts that the relationship between the meter output and the "true" void fraction (ϵ) is:

$$\text{Void meter output} = \left(\frac{3\epsilon}{2 + \epsilon} \right). \quad [2]$$

Despite the fact that bubble flow is a dynamic process in which the bubbles are rarely spherical, or uniform in size, or small compared to their spacing, and are not distributed homogeneously, [2] is frequently quoted as being representative of bubble flow. Merilo *et al.* (1977) showed that it compared well with their vertical flow measurements, made with quick-closing valves and a conductivity-based void meter. The trends in Merilo's data are very similar to those evident in figure 2, even though significantly different electrode geometries were employed.

The apparent agreement in figure 2 between the Maxwell curve and the high void fraction data can only be fortuitous, since bubble flow is known to break down at mean void fractions above about 0.3. Maxwell (1873) pointed out that the theory only applies when ϵ is a small fraction, thus

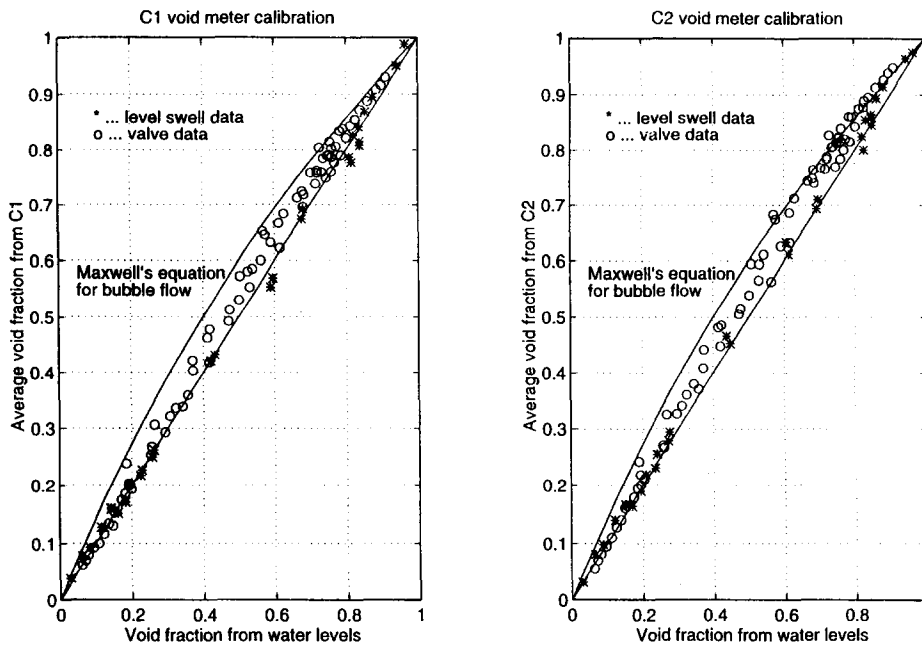


Figure 2. Calibration of conductivity meters.

the curve has no physical significance with void fractions of 0.5 and above. However, since most of the experimental data fall below this curve, but above a straight line, it has been included as a convenient reference.

In general the level swell data agree well with the void meter outputs, and agreement among all of the measurements is particularly good at void fractions below 0.3. Between 0.3 and 0.6 the meters may typically indicate values which are between 0.01 and 0.05 high. The most uncertain values occur in the 0.6 to 0.8 band of void fractions, with individual values being as much as 0.1 higher than quick-closing valves indicate. Above 0.8 the discrepancies are reduced, but indicated void fractions are still higher than the true values.

The quick-closing valve data are consistently lower than the void meters at higher void fractions. The biggest discrepancies all correspond to high liquid flow rates but they can be only partly accounted for by the tendency for the valve void fractions to be lower than the true value. The differences range up to 0.1 in void fraction. This level of agreement is considerably better than the 0.2 claimed by Ma *et al.* (1991) for similar measurements.

2.3. Void meter simulation

Considering the geometry of the electrodes it is not obvious why the nearly linear response displayed by the calibration data should be obtained: the fluid adjacent to the ends of the electrodes will be more sensitive to the presence or absence of voids than that occupying the remainder of the cross section, and significant errors might be expected as a result. The probe performance was therefore simulated mathematically, to investigate its sensitivity to void distribution.

For convenience the fluid dynamics code "Fluent" (Fluent Inc.) was used to model the conductance probe's behaviour by solving the steady heat conduction equation. The two electrodes were simulated by 160° arc boundaries maintained at different, constant temperatures, and the insulating part of the circular wall was a zero heat flux boundary. Voids were simulated by creating regions with adiabatic boundaries surrounding dead cells. Zero velocity was imposed to ensure a pure conduction solution. Since the temperatures and geometry of the boundaries were always constant, the heat fluxes entering at the hot wall and leaving at the cold wall were proportional to the conductance, c , of the probe; in most cases these values agreed to within 1 part in 1000.

A selection of the geometries investigated is shown in figure 3. Pure annular flow, distributed voids—approximating bubbly flow—and asymmetric void distributions were all considered. The conductance at zero void fraction, c_0 , was calculated. Then the steady state response for any void

distribution was given by the value $(1 - c/c_0)$. In figure 3 (a), (b) and (d) calculated equipotential lines are shown; they are omitted from figure 3 (c) since they tend to obscure the geometry.

Each calculation corresponds to an instantaneous response for a particular void distribution; for annular and bubbly flows whose void distributions are more or less consistent, this is representative of the time averaged value, but average values for asymmetric flows must be found from a number of calculations. The results of all of these calculations are summarised in figure 4.

2.3.1. *Void fraction in annular flow.* The pure annular flow results are shown for void fractions of 0.6 and above. The probe response is almost linear, but there is a tendency to underestimate the true void fraction. The actual probe response to annular flows can be seen in figure 2: for most void

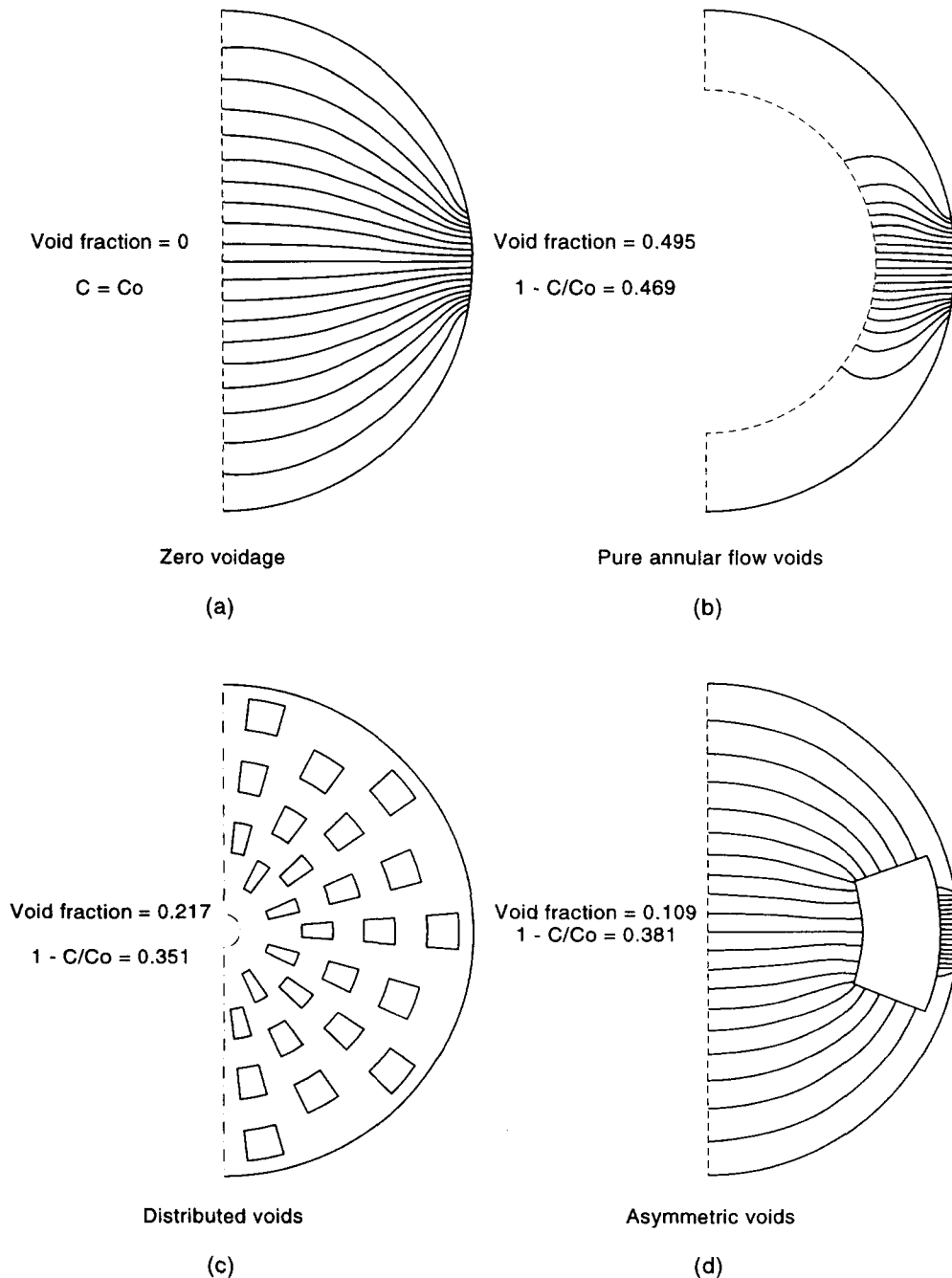


Figure 3. Simulation of different void distributions.

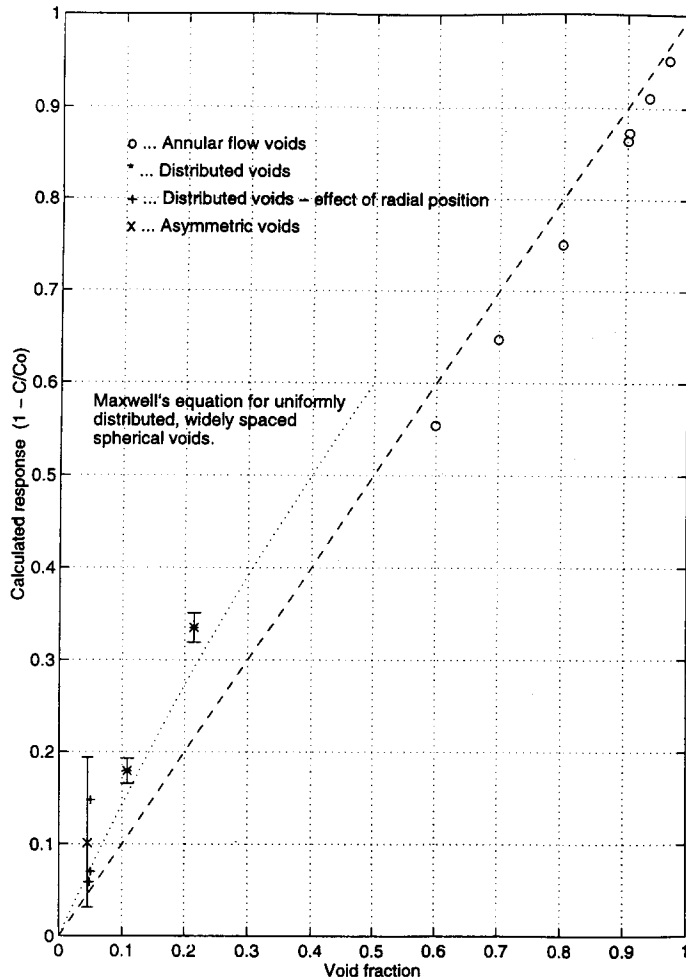


Figure 4. Numerical simulation of void meter response.

fractions the probe output is higher than the true value, not lower as predicted in figure 4. This behaviour is attributed to the presence of entrained liquid in real annular flows.

The liquid entrained in the gas core of an annular flow can be a significant fraction of the total liquid flow. However, it will not be detected by a conductivity meter. This means that the void fraction deduced from measurements on the wall film alone will always be higher than the true value. This effect can easily counteract the calculated tendency to underestimate the void fraction in pure annular flow.

2.3.2. Distributed voids. Several distributed void patterns were produced in cylindrical coordinates. The calculated meter responses were considerably higher than those predicted by the Maxwell equation for uniformly distributed voids. The vertical bars on each point in figure 4 show the extreme values calculated for different angular positions. The fact that the simulated voids are based on radial segments means that a larger proportion of the voidage is located at larger radii, close to the electrodes. The meter responds more to voids located near the electrodes than it does to those located near the tube centreline. This was demonstrated by calculating the response to a uniformly distributed void fraction of 0.05 located at different radii. When the voids were all between radii of 14 and 15 mm the calculated response was 0.148 and around the centreline in pure annular flow it was 0.059. At intermediate positions the calculated output increased with radius.

A meter output between the ideal linear response and the Maxwell curve for bubble flows is therefore possible if most of the voidage is concentrated around the tube centreline. The phenomenon of voidage peaking near the centreline in developed bubbly flows has been observed many times (Malnes 1966; Serizawa 1974), similar observations have been made in liquid slugs

during slug flow (van Hout *et al.* 1992). Taking this together with the possibility of finding calibration void fractions which are slightly low, the location of the bubbly flow data (say below a void fraction of 0.4) in figure 2 is entirely plausible.

2.3.3. Asymmetric void. A single void was positioned on an outer radius close to the mid point of one electrode; its response at this and six other azimuthal positions at 15° intervals was calculated. When the void bridged the ends of the two electrodes (figure 3 (d)) the calculated output was as much as four times greater than the actual void fraction, but the average of all seven values was closer to the results calculated for voids close to the boundaries.

The magnitude of the maximum overestimate of void fraction decreases as the individual asymmetric void increases: for example with a void fraction of 0.2 across the electrodes, the calculated response is 0.34. The response to voids larger than 0.5 will also be high, but since the maximum overestimate cannot exceed a value of 1.0, the average value will approach the true value as the void fraction increases.

2.3.4. Implications for slug and churn flows. It has been shown that the experimentally observed tendency of the meter to slightly overestimate bubbly and annular flow void fractions is consistent with the model predictions of its performance when bubble void peaking and liquid entrainment are taken into account. Slug flow consists of Taylor bubbles of varying lengths alternating with bubbly liquid slugs. Since the Taylor bubble is essentially annular flow with little or no entrainment, the void meter sees periods of pure annular flow alternating with periods of bubbly flow. The time average of its response to these flows is therefore likely to exhibit a near linear relationship to the mean void fraction, and individual values will be as accurate as they are in bubble or annular flow.

The flow patterns in which most asymmetry occurs are those in which aerated slugs collapse from time to time and their liquid contents fall or drain into the film of the following Taylor bubble, frequently with a swirling motion. These regimes are characterised by large oscillations in void fraction but only a small proportion of the data are expected to be below a void fraction of 0.5. Therefore the overestimates of void fraction are likely to be highest in this region (mean void fractions typically of 0.6 to 0.8), but the meter accuracy will improve at higher void fractions; which is consistent with the observations shown in figure 2.

3. EXPERIMENTS AND RESULTS

Pressure variations at the test section inlet can be large in two phase flows, particularly in slug and churn flows. This can affect the flow rate of the gas—and hence the flow pattern development—if particular care is not taken. In all of these experiments the test section inlet air flows were fixed by using a number of critical flow nozzles. Twelve interchangeable nozzles with diameters between 0.32 and 9.0 mm were used to produce constant mass flow rates of air, in increments between the bubble and annular flow regimes. These flows were measured by variable area flowmeters or standard orifice plates, measurements were corrected for air density variations.

Void meters C1 and C2 were positioned 5.050 m and 5.827 m respectively above the pressure transducer at the test section inlet. A thermocouple was installed 0.152 m above the second void meter and connected into the data logger to monitor the water temperature during a run.

Nine water flows (labelled “ra0” to “ra8”), and 12 air flows (corresponding to the 12 orifices—labelled “a” to “l”) were investigated. Thus void fraction measurements were made on a matrix of 9 by 12 data points. After tests at 800 Hz and 200 Hz, the logger sampling rate of 200 Hz was selected. Visual observation of the flow patterns suggested that slug frequencies were typically about 1 Hz, therefore, it was decided that a sampling time of 20 s would give an adequate picture of the flow.

All data processing started with the raw data which was four-point filtered to remove noise. Void fractions, their probability distribution functions and power spectral densities were routinely examined. In addition velocities of characteristic disturbances were calculated by cross correlation of the void meter signals, and, in a later series of 400 s duration tests, slug and bubble lengths were determined.

3.1. Typical results from each flow pattern

Six data points, taken at the same water flow, have been chosen to illustrate features of each flow pattern detected. Points ra6a, ra6c, ra6e, ra6h, ra6i and ra6l are shown in figure 5. Data from the C2 probe alone are shown in these diagrams. The first 3 s of each void fraction trace are shown, above this the value of the void fraction obtained by averaging all of the data over the 20 s of the data record is given; to the right the probability distribution function (PDF) of the measured void fractions is given.

3.1.1. Discrete bubble flow. This name avoids confusion with “dispersed bubble” flow, as used by Taitel *et al.* (1980). It refers to essentially the same type of flow, in which small bubbles are more or less uniformly distributed in the liquid continuum, with no coalescence. Taitel *et al.* claim that bubble flow of this type cannot exist in air–water systems in tubes with diameters less than 50 mm, unless superficial water velocities are above about 3 m/s. Visual, photographic and void fraction data from our 32 mm diameter tube, show that we observe it at superficial water velocities of 0.2 m/s and above.

A characteristic void fraction trace of this flow pattern is shown in figure 5. The PDFs of these traces are narrow single peaks which occur at void fractions between 0.06 and 0.4, depending upon the superficial velocities. Individual void fraction determinations rarely exceed 0.4, except at the highest liquid velocities where values up to 0.45 were measured. These observations are in broad agreement with the findings of Jones and Zuber (1975), Vince and Lahey (1982) and with the data reported by Wang *et al.* (1991), even though they used different geometries or tube diameters.

3.1.2. Spherical cap bubble flow. This type of flow was called “plug” flow by Wang *et al.* (1991), and it is grouped by them and by Taitel *et al.* (1980) into bubbly flow. It may be argued that to delineate it as a separate regime complicates the description of flow patterns unnecessarily, since it represents a transition region between bubbly and slug flow. However, its voidage characteristics are sufficiently distinct from those of bubble or slug flow to enable us to recognise and describe them; therefore, it is included, if only to point out areas where confusion in defining flow pattern boundaries may arise.

The typical void fraction trace of this regime shows irregular narrow peaks superimposed on the bubble flow trace. The peaks reach void fractions well above 0.4 but normally do not exceed 0.8. The PDF trace shows the single peak of bubble flow with a broadening tail extending to higher void fractions.

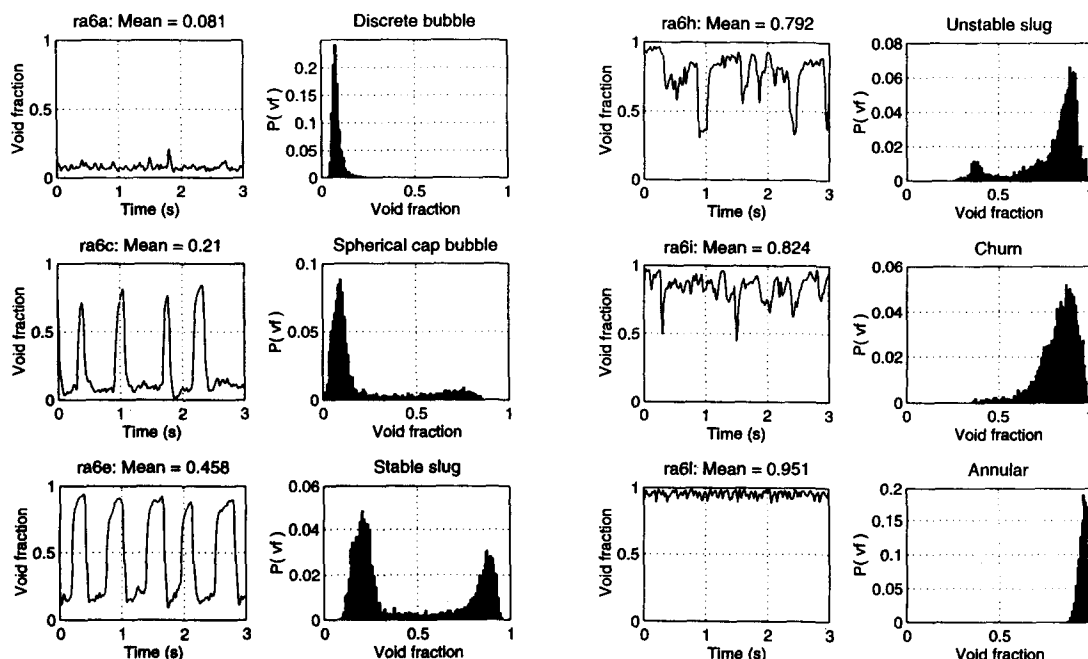


Figure 5. Typical void fraction traces and their PDFs.

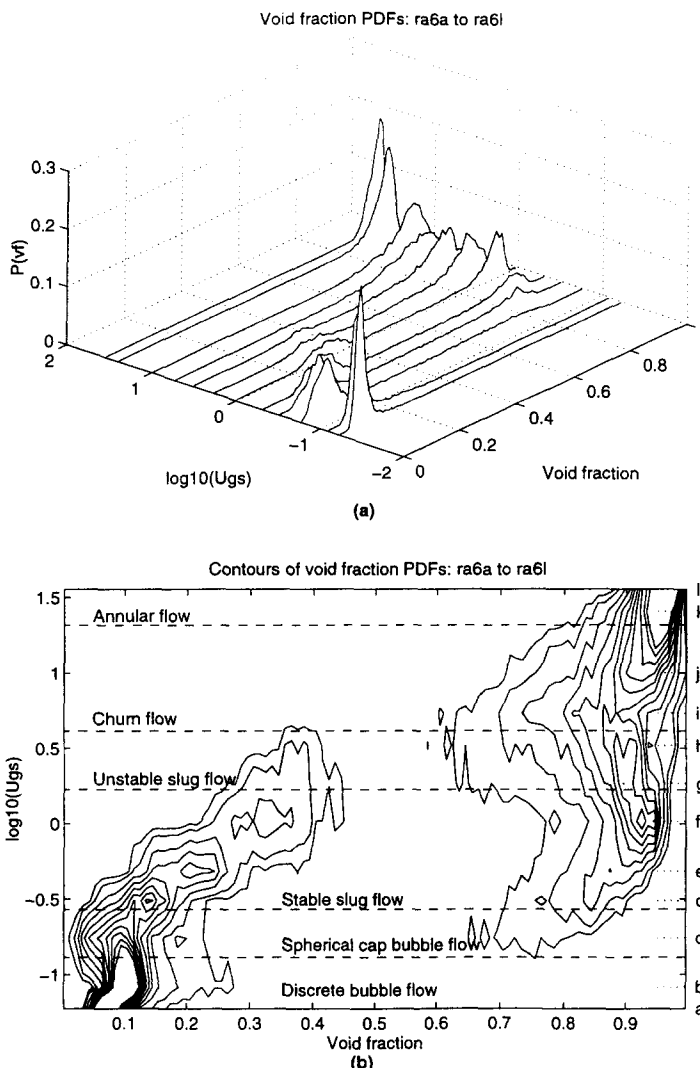


Figure 6. Void fraction PDFs and contours at constant water flow.

3.1.3. Stable slug flow. Stable slug flow extends over a wide range of liquid and gas velocities. Aerated liquid slugs are separated by Taylor bubbles of varying lengths. In most of the present data the Taylor bubbles have average void fractions greater than 0.8. The stable liquid slugs have mean void fractions between 0.3 and 0.42 (all of the data are below 0.45). The distribution of data in the twin peaks of the PDF moves from predominantly slug at low gas flows to predominantly Taylor bubble as the gas flow increases (see figure 6(a) and (b)). As this happens the void fractions in the liquid slug and the Taylor bubble both rise.

Void traces like that in figure 5 show how the liquid film thins and the bubble diameter increases away from the nose of the bubble. Occasionally ripples can be detected in the liquid film; these become more common as the gas flow increases. The liquid slugs all exhibit similar features; frequently a region of low void fraction exists at the front of the slug, the void fraction then tends to increase in an oscillatory manner with the slug length, up to maximum values of 0.35–0.45.

This behaviour is similar to that observed by van Hout *et al.* (1992) if the high void fraction bubble wake region they identify as part of the slug is disregarded. This is not meant to imply that such a region does not exist, indeed some transition between the high bubble void fraction and the low slug void fraction is to be expected. It is more a question of defining where the bubble ends and the slug begins. The presence of liquid on the pipe centreline in the highly turbulent wake region of a bubble does not, of itself, imply the existence of a liquid continuum. And it would be

inconsistent to suggest that bubbly flow can only exist at void fractions up to 0.45 and then to allow void fractions of up to 0.6 in liquid slugs. All of our measurements indicate that liquid slugs begin to collapse when their void fractions are in the 0.35–0.45 region, and that more than a few void fraction measurements in excess of 0.4 are indicative of the fact that slugs are collapsing.

Figure 6(b) shows that the gas velocity can be increased through the slug flow regime (points ra6d to g), until, between points ra6f and ra6k a discontinuity occurs. The slug void fraction exceeds 0.4 and slugs start to collapse. Aerated liquid falls in the tube causing the bubble void fraction to fall significantly. Violent oscillations appear, and some workers have identified this as the inception of churn flow. The cause of the discontinuity is discussed below, but we note here that it happens in the vicinity of point g (i.e. a gas velocity of about 1.9 m/s) for most water flows tested.

3.1.4. Unstable slug flow. The more chaotic nature of unstable slug flow is shown in figure 5. Here the mean void fraction is about 0.8, but the void fraction vs time trace has a ragged appearance, with frequent occurrences of voids below 0.4, occasional slug void fractions up to 0.45 are possible. The probability distribution shows a peak at a void fraction of 0.9, but with a long tail down to 0.3, which still exhibits the remains of a peak around 0.4.

If a slug collapses at high liquid flow rates (such as ra5 and above) the falling liquid is intercepted by a following slug, which may or may not collapse or fall itself. Thus, although some slugs are collapsing and there are obvious chaotic oscillations in the flow, other slugs still have sufficient momentum to traverse the length of the test section. It is difficult to decide whether to classify this type of flow as slug or as churn, since it exhibits some characteristics of both. But the name “unstable slug flow” conveys the fact that not all of the slug structure of the flow has broken down, even though individual slugs may appear only sporadically. This unstable slug region persists until the gas flow is high enough to break down all of the slugs and distribute their contents in the form of waves on an annular film. But even then the gas flow may still be too low to maintain stable annular flow, so oscillations of aerated liquid on the film surface persist into what is now the churn flow region.

3.1.5. Churn flow. We consider churn flow to be fundamentally annular in nature in which large disturbance waves are carried up the tube by the gas flow; the liquid film may continue to drain down the wall as in Taylor bubbles and occasionally the waves may bridge the tube or fall within it. The churn flow data in figure 5 show that the mean void fraction is now above 0.8, suggesting that the flow is primarily annular, but the liquid film thickness is erratic and shows large disturbances with void fractions down to less than 0.6.

3.1.6. Annular flow. Annular flow is well recognised and consists of a thin annular film of liquid on the tube wall on which small ripples, interspersed occasionally with larger disturbance waves, flow in a regular manner up the tube. In annular flow, our measured void fractions are always above 0.8 and usually above 0.9. The time trace shows high frequency components; a maximum of 12.4 Hz was found from the power spectrum, but there are also many more frequencies of comparable significance.

Similar diagrams to those in figure 5 have been plotted for all of the other data points, but lack of space precludes their inclusion. It is of interest, however, to examine how the distribution of void fraction changes as the gas flow is varied at a constant water flow. In figure 6(a) we have plotted the PDFs of data points ra6a to ra6l against the logarithm of gas velocity. As the gas velocity is increased they change from a single peak in bubble flow at a low velocity, through the twin peaks of slug flow into churn flow and end in the single high peak of annular flow. It is even more informative to study this data in the form of contour maps such as figure 6(b). The data points, whose PDFs form the cross sections of this plot, are labelled with the letter of the point along the right hand edge, beside short, dotted horizontal lines; thus the positions of the data from figure 5 can be identified.

The contours shown start at a probability of 0.005, the next contour is 0.01, each subsequent one is incremented by 0.01, up to a maximum of 0.1. The highest peaks in annular flow can go up to 0.8; but the presence of a peak is obvious and it is not necessary to obscure the plot with more lines than are shown. The significance of these contours is that they indicate the probability of occurrence of a particular void fraction; this does not give any information about what proportion of the data are enclosed by any contour, which is obtained from the cumulative probability. This information has been calculated separately for the first two contour lines; the

results show that the 0.005 probability line encloses 86% and the 0.01 line 74% of all of the data reported here.

3.2. Flow pattern identification from void fraction measurements

Six flow patterns have been identified by examination of void fraction traces, PDFs and PDF contours, similar to those in figures 5 and 6. We summarise our flow pattern identification criteria as follows:

Discrete bubble flow occurs with local void fractions which depend upon the gas and liquid velocities, but are at all times less than 0.45.

Spherical cap bubble flow consists of discrete bubble flow upon which irregular narrow void fraction peaks between 0.4 and 0.8 are superimposed.

Stable slug flow exists when liquid slugs with void fractions up to 0.4 are separated by Taylor bubbles with void fractions of 0.8 or more.

Unstable slug flow occurs at relatively high liquid velocities. It is characterised by slug void fractions which are higher than 0.4 merging with Taylor bubble void fractions which are lower than 0.8.

Churn flow exists when many of the bubble / annular void fractions are below 0.8, but there are no low void fraction slugs remaining.

Annular flow exists if all void fractions are above 0.8.

These void fraction flow regime transition criteria are best estimates from the data collected in this study. Applying the criteria to all of our data points gives the flow map shown in figure 7. The regime boundaries are indicated by dashed lines in figures 6(b) and 7. The methods of locating the two lines dividing the discrete bubble from the stable slug flow regimes in figure 7 are described in Costigan and Whalley (1996).

Since we allow discrete bubble flow with void fractions up to 0.45, and also claim that, at this void fraction, liquid slugs break down to form unstable slug flow, we might expect to see a direct transition from high void fraction discrete bubble flow to unstable slug flow. Point ra8f approaches this condition most closely, although it has been identified as spherical cap bubble flow to conform with the above criteria.

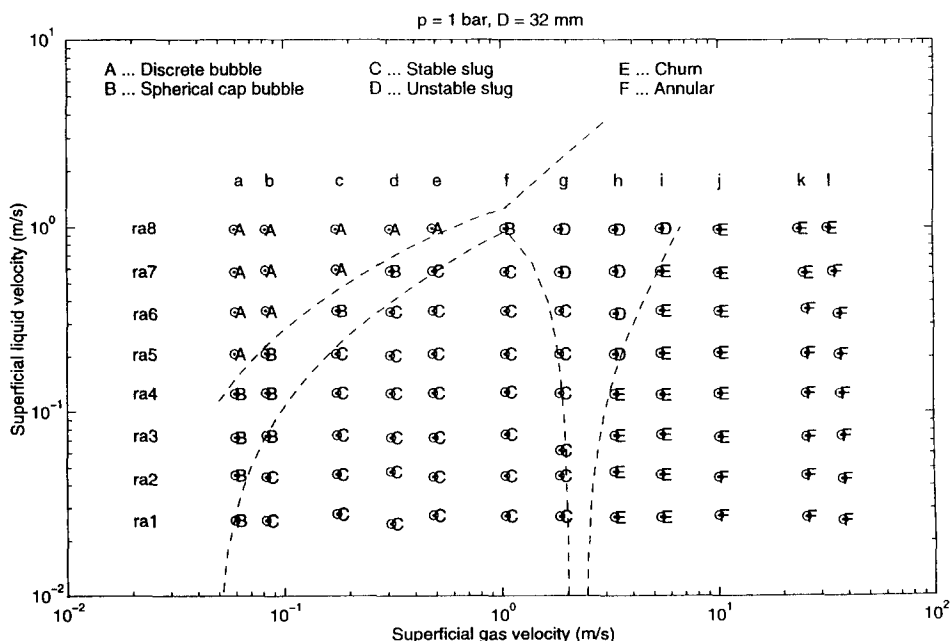


Figure 7. Data points on flow map.

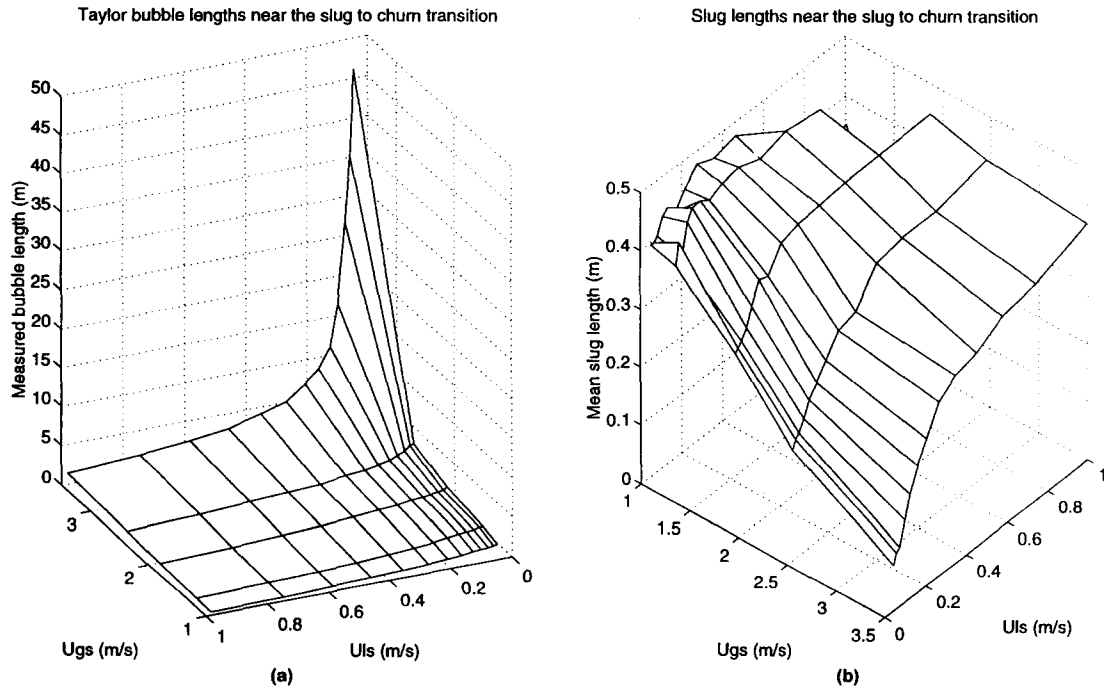


Figure 8. Mean bubble and slug lengths from 400 s runs.

3.3. Slug and bubble lengths

By cross-correlating the void fraction signals from C1 and C2, the transit time between the two meters can be measured; this together with the distance between the meters enabled us to calculate the velocity of the characteristic disturbances in the flow.

In the 400 s runs in which bubble and slug lengths were determined, the velocities were produced by cross-correlating the first fifty seconds of data. They thus represent an average velocity. Measurements made on shorter sections of the data record, reveal variations above and below this mean value. In general slug velocities determined by this method are in quite good agreement with the commonly accepted (see e.g. Nicklin 1962) correlation for slug velocity:

$$U_s = 1.2(U_{LS} + U_{GS}) + 0.35\sqrt{gD}. \quad [3]$$

Indeed the correlation makes reasonable velocity predictions for the spherical cap bubble and unstable slug flow data, for which it is not strictly applicable. The use of this expression to calculate the mean void fraction from the relationship:

$$\epsilon = \left(\frac{U_{GS}}{U_s} \right) \quad [4]$$

also gave adequate results.

Knowing the slug velocity makes it possible to estimate slug and bubble lengths from the void fraction time trace, provided that a criterion for the slug maximum (and Taylor bubble minimum) void fraction is adopted. This value was chosen to be 0.45 as indicated by the data (see, e.g. figure 6(b)).

A separate series of tests was carried out to examine slug and bubble lengths and void fractions in detail. The data cover the slug to churn transition region with superficial gas velocities between 1 and 10 m/s. To ensure that at least 250 slugs and Taylor bubbles were examined at each data point, 400 s of data were recorded. This meant that the mean lengths were accurate to within $\pm 5\%$, assuming a normal distribution.

In stable slug flow the bubble and slug lengths were approximately normally distributed, with standard deviations typically 40–50% of the mean value. Average Taylor bubble lengths and

average slug lengths are summarised in figure 8(a) and (b), respectively, as surface plots; the intersections of the mesh lines indicate data points. The corresponding contour plots derived from these surfaces are shown in figure 9(a) and (b). The dramatic rise in bubble length and the corresponding fall in slug length in churn flow can be seen. Apparently unreasonably high bubble lengths of tens of metres merely indicate that the instrumentation has not observed a void fraction of less than 0.45 in the time period which would correspond to the passage of a bubble of that length—a fairly reliable indicator of the existence of churn flow. More measurements were made at higher gas velocities, but, except at high liquid velocities, the rapid development of churn flow led to the bubble lengths becoming extremely high and their numbers too small to provide any confidence in them.

The maximum slug length observed was 15 diameters; most of the stable slugs had a mean length of 12 diameters, and slug collapse appeared to increase dramatically at lengths less than eight diameters. Stable slug void fractions varied most with gas velocity between 0.3 and 0.42, the mean value for all of the stable slugs was 0.35.

4. SLUG FLOW REGIME BOUNDARIES

The ways in which the slug flow boundaries, drawn in figure 7, were defined are set out in the following paragraphs.

4.1. Stable slug flow to unstable slug flow

Figure 6(b) and similar contour plots illustrate our concept of stable and unstable slug flows in terms of void fraction distributions: as mean slug void fractions approach and exceed 0.4 the Taylor bubble void fraction peak falls and considerable decreases in bubble void fraction become apparent. This is symptomatic of the appearance of large waves on the Taylor bubble film (see the unstable slug flow void trace in figure 5), and a redistribution of the liquid content of many slugs. This and the collapse of some of the shortest slugs give the flow its chaotic appearance.

It has already been pointed out that the model of Mishima and Ishii (1984) predicts the opposite trend to that observed for this transition, but even if this were not the case, our measurements do

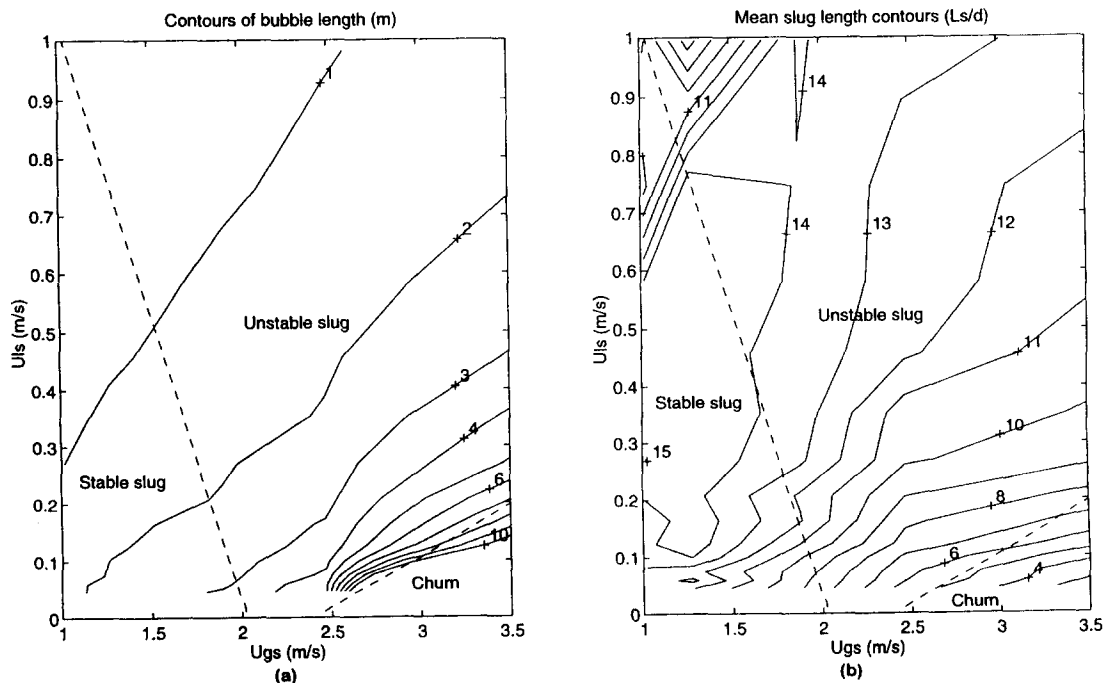


Figure 9. Mean bubble and slug length contours.

not bear out their basic assumption that slug void fractions (maximum measured value 0.43) approach average void fractions (minimum measured value 0.6) at the transition.

The Brauner and Barnea (1986) criterion predicts transition gas velocities which are too high compared with our data, but it is based upon a transition slug void fraction of 0.52, which is higher than any we measured. If the average, measured, stable slug void fraction of 0.35 is used instead of 0.52, then Brauner and Barnea's equation [1] gives a better representation of our transition boundary, but the gas velocities are still slightly high. The data show that this transition occurs over a narrow range of void fraction about 0.38, this suggests that Brauner's equation [1] (after Taitel *et al.* 1980) can represent lines of constant slug void fraction. But it does not give any indication of what causes slug collapse, since we observe other slugs in the unstable region with mean void fractions up to 0.43.

The Taitel *et al.* (1980) suggestion that slug flow requires an entry length in which to stabilise, depends upon the observation that the second of two, successive, closely-spaced Taylor bubbles tends to travel faster than the first, and to accelerate as the distance between them diminishes (Moissis and Griffith 1962). Thus if the slug between two bubbles is not long enough to ensure that the wake of the first bubble does not influence the speed of the second, both bubbles will ultimately collide and amalgamate. The stable slug separation length is claimed to be $16D$. By assuming that the slug void fraction is constant at 0.25, and starting with a very short slug, Taitel estimated the time required to form a slug of length $8D$ (chosen because the time required to double the slug length from $8D$ to $16D$ would be excessive). The entry length needed to form slugs of this length was then a function of the Taylor bubble rise velocity, which in turn depended on the gas and liquid superficial velocities. At all mixture velocities up to that which makes the observation point equal to the entry length, the slug flow will appear stable, since bubble coalescence will occur only infrequently. Whereas at higher mixture velocities slug collapse and bubble coalescence will be observed much more frequently, giving a chaotic appearance which Taitel describes as churn flow.

By substituting our mean slug void fraction (0.35) into Taitel's theory, the results for the position at which the void fraction measurements were made (5.827) separate our stable and unstable slug flow data well, and coincide with the modified Jayanti and Hewitt transition line (see section 4.2) at low liquid velocities.

The slug length contours of figure 9(b) show a more even distribution in the stable slug flow region (about $10D$ – $15D$), than in the unstable slug flow region (about $7D$ – $14D$), which tends to support the Taitel model. But when the number of bubble coalescences which occurred between meters C1 and C2 was determined from the 400 second run records, values of 11, 16 and 10 were found for points equivalent to ra6f, ra6g and ra6h, respectively. The minimum number of bubbles observed in this comparison was 466, therefore the evidence of increased bubble coalescence frequency as the transition boundary is crossed is not convincing. It is certainly the case that a minimum entry length is required to establish stable slug flow, but all of our measurements suggest that stable slugs have been formed at the level of meter C1. therefore, the minimum entry length criterion's agreement with our data appears to be fortuitous.

Niklin and Davidson (1962) were the first to suggest that flooding in the liquid film near the base of a Taylor bubble is the cause of the slug to churn flow transition. Hewitt and Wallis (1963) subsequently showed that Niklin and Davidson's data could be correlated using Wallis's (1961) flooding criterion:

$$\sqrt{U_{Gs}^*} + \sqrt{U_{Ls}^*} = C \quad [5]$$

where the value of C was found to be 1.0.

In general, conditions at the bottom of a falling liquid film are believed to govern the inception of flooding: with sufficient turbulence a wave can easily form and grow on the film, causing the film flow from above it to be reduced. The shear layer formed as the film at the base of a Taylor bubble enters the liquid slug will ensure conditions of high turbulence, promoting the formation of such entry-type flooding waves if the relative velocity between the gas and liquid is high enough. When this flooding point is reached, the bubble film will become thicker since liquid is unable to drain from it at the same rate as before flooding. Large waves may buildup on the film and subsequently fall. The following slug will be starved of liquid inflow, its length will fall and its void

Table 1. Slug and bubble parameters in stable and unstable flow regimes

Run	l _{xe} a + ra6f		l _{xe} c + ra6g		l _{xe} e + ra6h	
Slug unit velocity (m/s)	1.671		2.825		5.18	
Sample size	513		548		466	
	Slugs	Bubbles	Slugs	Bubbles	Slugs	Bubbles
Mean length (m)	0.468	0.834	0.433	1.626	0.318	4.124
Standard deviation (m)	0.196	0.285	0.243	0.726	0.213	2.171
Mean void fraction	0.302	0.846	0.35	0.821	0.394	0.792

fraction will rise; if this slug is very short it will collapse and allow two bubbles to coalesce. We would therefore expect to see evidence of the following events as the gas velocity is increased at constant liquid velocity from the stable to the unstable slug flow regime: first the bubble velocity and length would rise to accommodate most of the increased gas flow; the liquid film around the bubble would have large irregular waves on it which reduce the mean void fraction of the bubble; the mean slug length would decrease and its void fraction would increase due to the increasing liquid hold up in the bubble film; the number of slugs would gradually fall as the shortest ones were depleted of liquid and broken up. This is the sequence of events which emerges from studying the bubble and slug length data. Table 1 shows data for conditions equivalent to runs ra6f, ra6g and ra6h respectively, which support this interpretation.

McQuillan and Whalley (1985) calculated the gas velocity in the bubble and the liquid velocity in the film, by simultaneous solution of the continuity equation and Nusselt's equation for the thickness of a laminar falling film. They then used [5] with $C = 1.0$ as the transition criterion. Their results predict lower transition gas velocities as the liquid flow is increased. The line shown in figure 7 was derived from the McQuillan and Whalley model, using the Brotz (1954) film thickness expression for turbulent liquid films, as suggested by Jayanti and Hewitt (1992). The stable and unstable slug regimes are well separated by this line.

4.2. Unstable slug flow to churn flow

Churn flow consists of a chaotic annular type of flow which has many instantaneous void fractions well below 0.8, but does not exhibit the presence of a slug void fraction peak around 0.4. The data show that the transition boundary to this regime moves to higher gas velocities as the liquid flow is increased. The Taylor bubble length data of figure 8(a) also display this trend.

We believe that this transition is also brought about by a form of flooding in the liquid film surrounding long Taylor bubbles but that it is of a different kind to the inlet flooding which causes the slug flow transition.

Hewitt (1982) pointed out that flooding data fall into two groups. In the first group the entry conditions are dominant and flooding waves are formed near the inlet with relatively low gas velocities, no effect of the length of the falling film can be found in these results. The second group of data was obtained by Hewitt *et al.* (1965); by careful control of the inlet conditions they showed that waves grew on the liquid film as they travelled upwards, and that larger gas velocities were required to initiate flooding in a short liquid film than in a long one. It is this second type of flooding, which will only occur if the liquid film (Taylor bubble) is long enough and the gas velocity is high enough, which finally destroys the remaining slug structure and leads to churn flow.

Jayanti and Hewitt (1992) substituted the equation proposed by Brotz (1954) for the Nusselt equation, to find the film thickness in the McQuillan and Whalley calculation, and proposed that the flooding criterion should be:

$$\sqrt{U_{gs}^*} + m\sqrt{U_{ls}^*} = C. \quad [6]$$

They derived m from the Hewitt *et al.* (1965) flooding data as a function of liquid film length. In their calculation they assumed a constant slug length of $12D$ and a slug void fraction of 0.5 to calculate the bubble length, enabling m to be found.

When our unstable slug to churn data were compared to the Jayanti and Hewitt prediction the correct trend was found, but the prediction did not fit our measurements closely. The most obvious disagreement with our data was that the lengths calculated for the Taylor bubbles were considerably less than the corresponding measured mean values. In addition the inlet and exit conditions of the counter-current flooding experiments of Hewitt *et al.* (1965), on which the correlation for m is based, were significantly different from the closed ends of a Taylor bubble. It may be that the “film only” flooding data require adjustment to predict flooding in the rather different hydrodynamic conditions of slug flow. We therefore made the following modifications to the model. The stable slug length of $12D$ was retained but the measured average slug void fraction of 0.35 was used instead of 0.5. The velocity of the liquid in a stable slug was taken as the slug velocity given by [3], rather than the mixture velocity and m was calculated from:

$$m = 1 - \exp \left\{ - \left[\frac{\left(\frac{L}{D} \right)^2}{60} \right] \right\} \quad [7]$$

which agrees closely with Jayanti and Hewitt’s equation for values of (L/D) of 60 and above, but falls to zero when $(L/D) = 0$. The results are shown on the flow map in figure 7; good agreement with the measured transition velocities has now been achieved, and the calculated bubble lengths have been increased to between 1.5 and 3.0 m, but they are still shorter than the corresponding measured values. Bearing in mind the large variation in measured bubble lengths, it is possible that, as these transition conditions are approached, some bubbles experience flooding while others remain too short. This would effectively increase the average length values. Another possible reason for the discrepancy is that the obstruction free inlet and exit conditions set up by Hewitt *et al.* (1965) in their flooding experiments, are not achieved in slug flow until even longer Taylor bubbles are formed.

Jayanti and Hewitt’s maximum bubble length (by comparison with flooding length data) is $(L_b/D) = 120$ which is 3.84 m for our experiments. Their formulation of the flooding criterion thus requires a minimum Taylor bubble length of about 4 m before the value of m is 1.0 and [6] becomes equivalent to [5]. Figures 8(a) and 9(a) show that stable bubbles much longer than 4 m are unlikely to occur in our system, since they are near the churn flow boundary; any increase in gas flow leads to longer bubbles which flood, producing churn flow. Thus it appears that satisfying [5] as well as the minimum bubble length condition may not be possible in practice.

5. DISCUSSION

The evidence for the existence of the unstable slug flow regime is compelling. Many workers have identified it visually and sought to establish the transition boundary at the edge of the stable slug flow regime. They have tended to describe the subsequent flow pattern as churn or froth flow. Mao and Dukler, on the other hand, recognised the obvious instabilities in this region, but pointed out its essentially slug like characteristics. By defining unstable slug flow as separate from churn flow it is possible to reconcile both points of view: to describe churn flow as occurring when the bubble or slug structure is disrupted is less precise than our definitions, which are based on void fraction, and has led to confusion over the correct location of the transition line.

The success of what appears to be the same equation in predicting two transition lines, both arising from flooding based phenomena, is at first surprising. It is necessary to acknowledge that two different types of flooding behaviour are being described, the first of which sets up the conditions for the second to occur. The slug and bubble length measurements (figures 8 and 9) show that bubble lengths increase and slug lengths fall gradually, as the gas flow is increased in the unstable slug flow regime. But when the churn flow boundary is reached their rates of change increase dramatically. We conclude from this that the instabilities observed in unstable slug flow are caused by a gradual, progressive process.

As the gas flow increases the void fraction traces show that stable Taylor bubbles become longer and ripples appear on their surfaces. The formation of large waves on the liquid film near the base

of the bubbles is characteristic of the transition to unstable slug flow. This was what Nicklin and Davidson suggested was happening as a result of flooding. As we have seen, [5] on its own predicts transition to unstable slug flow with a superficial gas velocity of about 2 m/s at low liquid flows, which falls to about 1 m/s at high liquid flows, and it has been found to fit the transition data of Nicklin and Davidson. We reiterate that no length of bubble is specified in the solution of [5] since it refers to the initiation of flooding near the base of a bubble. The formation of waves on the films surrounding lengthening bubbles persists until a combination of bubble length and gas flow is reached which will satisfy [6].

The modified version of the Jayanti and Hewitt theory describes the final stage of slug breakdown to churn flow as a consequence of flooding conditions which arise on long liquid films. Flooding in a long bubble will restrict still further the downflow of liquid into the following slug (which has already had its length reduced and void fraction increased to critical levels), the slug will continue to drain around the bubble following it at the same rate as before. Therefore the slug void fraction will rapidly rise to a level (say 0.45) at which coalescence of the small bubbles in the slug is inevitable. The slug then disintegrates, shedding its remaining liquid and forming a longer bubble. This longer bubble is even more prone to flooding at this gas flow and the remaining slug structure rapidly degenerates into churn flow, in which the "bubbles" become very long, as figure 8(a) illustrates.

The explanations offered above to account for the inception of unstable slug flow and churn flow are consistent with all our measurements. They are based upon the occurrence of two different types of flooding behaviour, both of which have been observed experimentally. They are in close agreement with the findings of other workers, and apparently divergent views about what constitutes churn flow can be reconciled by them. It would not have been possible to differentiate between these two types of flow without the insight provided by examination of the dynamic void fraction records produced by the conductivity meters.

6. CONCLUSIONS

1. An existing design of conductivity based void fraction meter has been developed, tested and shown to be accurate to within ± 0.1 over the whole range of void fraction.
2. Two of these meters have been used together to record dynamic void fractions at 108 data points (covering water superficial velocities from 0 to 1.0 m/s and air superficial velocities from 0.05 to 37 m/s in a 32 mm diameter tube).
3. Constant air flows were ensured by using critical flow nozzles at the test section inlet.
4. Void fraction records show fully developed slug flow at 5.0 m above the inlet.
5. Examination of void fraction traces and their probability distribution functions enabled the following six flow regimes to be identified: discrete bubble flow, spherical cap bubble flow; stable slug flow; unstable slug flow; churn flow; annular flow.
6. Cross-correlation of the void meter signals has provided statistical data on slug and bubble lengths and void fractions.
7. As gas flow is increased at constant liquid flow, Taylor bubble lengths increase but their void fractions fall. slug lengths gradually decrease and their void fractions rise.
8. As liquid velocity is increased at constant gas velocity bubble lengths decrease with approximately constant void fractions. Slug lengths and void fractions tend to remain constant but the number of slugs and bubbles increases at the same rate as the bubble length falls.
9. Two different flooding mechanisms are identified with the transitions to unstable slug flow and churn flow. These transitions are well described by modifications to the McQuillan and Whalley (1985) and the Jayanti and Hewitt (1992) models, respectively.

Acknowledgement—This work was supported by the UK Engineering and Physical Sciences Research Council (EPSRC).

REFERENCES

- Albrecht, R. W., Crowe, R. D., Dailey, D. J., Damborg, M. J. and Kosaly, G. (1982) Measurement of two-phase flow properties using the nuclear reactor instrument. *Prog. Nucl. Energy* **9**, 37–50.

- Barnea, D., Luninski, Y. and Taitel, Y. (1983) Flow pattern in horizontal and vertical two phase flow in small diameter pipes. *Can. J. Chem. Eng.* **61**, 617–620.
- barnea, D., Shoham, O. and Taitel, Y. (1980) Flow pattern characterisation in two phase flow by electrical conductance probe. *Int. J. Multiphase Flow* **6**, 387–397.
- Brauner, N. and Barnea, D. (1986) Slug/churn transition in upward gas–liquid flow. *Chem. Eng. Sci.* **41**, 159–163.
- Brotz, W. (1952) Über die Vorausberechnung der Absorptionsgeschwindigkeit von Gasen in stromenden Flüssigkeitsschichten. *Chem. Ing. Tech.* **26**, 470.
- Costigan, G. and Whalley, P. B. (1996) Dynamic void fraction measurements in vertical air–water flows. Oxford University Report OUEL 2093/96.
- Danel, F. and Delhaye, J. M. (1971) Optical method for the measurement of local voids in two phase flow. *Measures* **99–101**.
- Fernandes, R. C., Semiat, R. and Dukler, A. E. (1983) Hydrodynamic model for gas–liquid slug flow in vertical tubes. *AIChE J.* **29**, 981–989.
- Harmathy, T. Z. (1960) Velocity of large drops and bubbles in media of infinite or restricted extent. *AIChE J.* **6**, 281.
- Hewitt, G. F. (1982) Flow regimes. *Handbook of Multiphase Systems*, ed. G. Hetsroni. Hemisphere Publ. Corp., New York.
- Hewitt, G. F., Lacey, P. M. C. and Nicholls, B. (1965) Transitions in the film flow in a vertical tube. *Proc. Symp. on Two-phase Flow*, Exeter, UK, 2, B401–B430.
- Hewitt, G. F. and Wallis, B. G. (1963). Flooding and associated phenomena in falling film flow in a tube. *Proc. ASME Multi-phase Symp. Philadelphia*, p. 62.
- Jayanti, S., Hewitt, G. F., Low, D. E. F. and Hervieu, E. (1993) *Observation of flooding in the Taylor bubble of co-current upwards slug flow. Int. J. Multiphase Flow* **19**, 531–534.
- Jayanti, S. and Hewitt, G. F. (1992) Prediction of the slug-to-churn flow transition in vertical two-phase flow. *Int. J. Multiphase Flow* **18**, 847–860.
- Jones, O. C. and Zuber, N. (1975) The interrelation between void fraction fluctuations and flow patterns in two-phase flow. *Int. J. Multiphase Flow* **2**, 273–306.
- Kondic, N. D. and Lassahn, G. D. (1978) Nonintrusive density distribution measurements in dynamic high temperature systems. *24th International Instrumentation Symposium*, Albuquerque, NM.
- Kosaly, G., Albrecht, R. W., Crowe, R. D. and Dailey, D. J. (1982) Neutronic response to two-phase flow in a nuclear reactor. *Prog. Nucl. Energy* **9**, 23–36.
- Ma, Y. P., Chung, N. M., Pei, B. S. and Lin, W. K. (1991) Two simplified methods to determine void fractions for two-phase flow. *Nucl. Technol.* **94**, 124–133.
- Malnes, D. (1966) Slip ratios and friction factors in the bubble flow regime in vertical tubes. Rep no KR-110 Inst. Atomenergei, Kjeller, Norway.
- Mao, Z. S. and Dukler, A. E. (1993) The myth of churn flow? *Int. J. Multiphase Flow* **19**, 377–383.
- Maxwell, J. C. (1873) *A Treatise on Electricity and Magnetism*. Clarendon Press, Oxford.
- McQuillan, K. W. and Whalley, P. B. (1985) Flow patterns in vertical two-phase flow. *Int. J. Multiphase Flow* **11**, 161–175.
- Merilo, M., Dechene, R. L., and Cichowlas, W. M. (1977) Void fraction measurement with a rotating electric field conductance gauge. *ASME J. of Heat Transfer* **99**, 330–332.
- Mishima, K. and Ishii, M. (1984) Flow regime transition criteria for upward two-phase flow in vertical tubes. *Int. J. Heat and Mass Transfer* **27**, 723–737.
- Moissis, R. and Griffith, P. (1962) Entrance effects in a two-phase slug flow. *ASME J. of Heat Transfer* **84**, 29.
- Nicklin, D. J. and Davidson, J. F. (1962) The onset of instability in two-phase slug flow. I. *Mech. E. Symposium on Two-phase Fluid Flow*, London.
- Serizawa, A. (1974) Fluid dynamic characteristics of two-phase flow. Ph. D. thesis, Kyoto University.
- Spindler, K. (1994) Void fraction distribution in two-phase gas–liquid flow in inclined pipes. *Proc. 10th Int. Heat Transfer Conf.*, Brighton, paper 14-TP-21.
- Taitel, Y., Barnea, D. and Dukler, A. E. (1980) Modelling flow pattern transitions for steady upward gas–liquid flow in vertical tubes. *AIChE J.* **26**, 345–354.

- Van Hout, R., Shemer, L. and Barnea, D. (1992) Spatial distribution of void fraction within a liquid slug and some other void related slug parameters. *Int. J. Multiphase Flow* **18**, 831–845.
- Vince, M. A., and Lahey, R. T. (1982) On the development of an objective flow regime indicator. *Int. J. Multiphase Flow* **8**, 93–124.
- Wallis, G. B. (1961) Flooding velocities for air and water in vertical tubes. UKAEA Report AEEW-R123.
- Wang, Y. W., Pei, B. S. and Lin, W. K. (1991) Verification of using a single void fraction sensor to identify two-phase flow patterns. *Nucl. Technol.* **95**, 87–94.